International Journal of Multiphase Flow 36 (2010) 780–792

Contents lists available at ScienceDirect

International Journal of Multiphase Flow

journal homepage: www.elsevier.com/locate/ijmulflow

Enhanced nucleate boiling on copper micro-porous surfaces

Mohamed S. El-Genk [a,b,c,*,1], Amir F. Ali [a,c]

[a] Institute for Space and Nuclear Power Studies, University of New Mexico, Albuquerque, NM, USA
[b] Chemical and Nuclear Engineering Department, University of New Mexico, Albuquerque, NM, USA
[c] Mechanical Engineering Department, University of New Mexico, Albuquerque, NM, USA

ARTICLE INFO

Article history:
Received 26 February 2010
Received in revised form 24 June 2010
Accepted 26 June 2010
Available online 7 July 2010

Keywords:
Nucleate boiling enhancement
Dendrites micro-structure
Micro-porous
Electrochemical deposition
Immersion cooling of electronics
Dielectric liquids

ABSTRACT

Saturation boiling of PF-5060 dielectric liquid on Cu micro-porous surface layers (95, 139, 171, 197 and 220-μm thick) is investigated. These layers are deposited on 10 × 10 mm Cu substrates using two-stage electrochemical process. The basic micro-structure, obtained in the first stage using current density of 3 A/cm^2 for 15–44 s, depending on thickness, is strengthened by continuing electrochemical deposition using much lower current density for 10's of minutes. For conditioned surface layers, after a few successive boiling tests, the pool boiling curves are reproducible and the temperature excursion prior to boiling incipience is either eliminated or reduced <7 K. Present nucleate boiling results are markedly better than those reported for dielectric liquids on micro- and macro-structured surfaces. Present values of CHF (22.7–27.8 W/cm^2) and h_{MNB} (2.05–13.5 W/cm^2 K) are ~40–70% higher than and >17 times those reported on plane surfaces (<16 W/cm^2 and ~0.8 W/cm^2 K). Best results are those of the 171-μm thick layer: CHF of 27.8 W/cm^2 occurs at ΔT_{sat} of only 2.1 K and h_{MNB} of 13.5 W/cm^2 K occurs at ΔT_{sat} = 2.0 K.
© 2010 Elsevier Ltd. All rights reserved.

1. Introduction

Immersion cooling of high power computer chips and central processing units (CPUs) using nucleate boiling of dielectric liquids on roughened, micro- and macro-structured, micro- and macro-porous and micro- and macro-finned surfaces, metal foam, macro-porous graphite and surfaces with reentrant cavities and macro-porous coatings has been the subject of numerous investigations for more than two decades (e.g., Kim et al., 2007, 2008; Chih et al., 2007; El-Genk and Parker, 2008; Li et al., 2008; Nimkar et al., 2006; Rainey and You, 2000; Parker and El-Genk, 2005, 2006, 2009; Vemuri and Kim, 2005; Yu et al., 2006; El-Genk and Bostanci, 2003; Chang et al., 1998; Webb, 2004; Jung and Kwak, 2006; Kim, 2006, 2009; El-Genk and Ali, 2010a,b; Xu et al., 2009; Albertson, 1977; Launay et al., 2006; Shin and Liu, 2004; Furberg, 2006; Wei and Honda, 2003; Ghiu, 2007; Sriraman and Banerjee, 2007; Chang and You, 1996; Jiang et al., 2001; Rajalu et al., 2004; Ramaswamy et al., 2003; Yu and Lu, 2007). These investigations attempted to demonstrate increases in both the Critical heat Flux, CHF, and the nucleate boiling heat transfer coefficient, h_{NB}, decreasing the corresponding surface superheats, and reducing or eliminating the excursion in surface temperature before initiating nucleate boiling. Temperature excursion is caused by the very low surface tension (<12 mN/m) of the highly wetting dielectric liquids, e.g., FC-72, PF-5060, and HFE-7100 (3M, 2009a,b,c). On plane copper and silicon surfaces, temperature excursions of as much as 25 K have been reported (Rainey and You, 2000; Parker and El-Genk, 2005; El-Genk and Bostanci, 2003; Chang et al., 1998; Jung and Kwak, 2006), which are highly undesirable since junction temperature could exceed the industry recommended value (<85 °C) for most chips.

The ever increasing transistor density and processing speed have increased the rate of thermal energy dissipation by a typical 10 × 10 mm chip up to 100 W and resulted in local hot-spots on the surface. The temporal variation on the chip surface could be as much as 10 °C, or even higher, and the hot-spots' local heat flux (>100 W/cm^2) could be 2–3 times the average value. The induced thermal stresses could eventually compromise the integrity of the chip, increasing failure frequency and reducing service life. Thus, desirable features for enhanced cooling of computer chips and CPUs, which could be realized using nucleate boiling of dielectric liquids are: (a) increasing the removal rate of dissipated heat, while maintaining a reasonable junction temperature, (b) reducing the number and local heat flux and temperature of the hot-spots by increasing the uniformity of surface temperature and the heat transfer coefficient for removing the dissipated heat and (c) reducing or eliminating the excursion in surface temperature prior to initiating nucleate boiling. These challenges may be dealt with effectively using micro- and macro-porous and structured surfaces (e.g., Kim et al., 2007, 2008; Chih et al., 2007; El-Genk and Parker, 2008; Li et al., 2008;

* Corresponding author at: Institute for Space and Nuclear Power Studies, University of New Mexico, Albuquerque, NM, USA. Tel.: +1 505 277 5442.
E-mail address: mgenk@unm.edu (M.S. El-Genk).
[1] Regents' Professor of Chemical, Nuclear and Mechanical Engineering and Director, Institute for Space and Nuclear Power Studies.

0301-9322/$ - see front matter © 2010 Elsevier Ltd. All rights reserved.
doi:10.1016/j.ijmultiphaseflow.2010.06.003

Nimkar et al., 2006; Rainey and You, 2000; Parker and El-Genk, 2005, 2006, 2009; Vemuri and Kim, 2005; Yu et al., 2006; El-Genk and Bostanci, 2003; Chang et al., 1998; Webb, 2004; Jung and Kwak, 2006; Kim, 2006, 2009; El-Genk and Ali, 2010a,b; Xu et al., 2009; Albertson, 1977; Launay et al., 2006; Shin and Liu, 2004; Furberg, 2006; Wei and Honda, 2003; Ghiu, 2007; Sriraman and Banerjee, 2007; Chang and You, 1996; Jiang et al., 2001; Rajalu et al., 2004; Ramaswamy et al., 2003; Yu and Lu, 2007).

For immersion cooling by nucleate boiling of dielectric liquids, CHF is a practical limit not to exceed, however, nominal operation is preferable at or near the maximum nucleate boiling heat transfer coefficient, h_{MNB}, occurring near the end of the fully-developed nucleate boiling region (II in Fig. 1). It is much higher than at CHF and the corresponding surface temperature or superheat is also lower (e.g., El-Genk and Parker, 2008; Rainey and You, 2000; Parker and El-Genk, 2005,2006; El-Genk and Bostanci, 2003; Chang et al., 1998; El-Genk and Ali, 2010a,b). A typical pool boiling curve of a dielectric liquid can be divided into four successive regions (Fig. 1): *(a) natural convection* up to the heat flux for the incipience of nucleate boiling, *(b) discrete-bubbles nucleate boiling* (region I) at low nucleate boiling heat flux and relatively low surface superheats; *(c) fully-developed nucleate boiling* (region II) at higher heat flux and slightly higher surface superheats and (*d*) *bubbles coalescence nucleate boiling* (region III), at higher heat flux and surface superheats than in region II, ending with CHF.

In the discrete-bubbles region (I), the nucleate boiling heat transfer coefficient increases with increased surface temperature, as more bubbles nucleation sites become active. In the fully-developed nucleate boiling region (II), the density of the active nucleation sites as well as the heat transfer coefficient are highest, as indicated by the steepest slope of the pool boiling curve (Fig. 1). The maximum nucleate boiling heat transfer coefficient, h_{MNB}, occurs near the end of region (II) and before transitioning to region (III). In region (III), the nucleate boiling heat transfer coefficient, $h_{NB,}$ decreases with increased surface superheat because of the added heat transfer resistance by the coalescence of growing and rising bubbles at and near the surface, until reaching CHF. Thus, at CHF, the nucleate boiling heat transfer coefficient is lower and the corresponding surface temperature, T_w, and surface superheat,

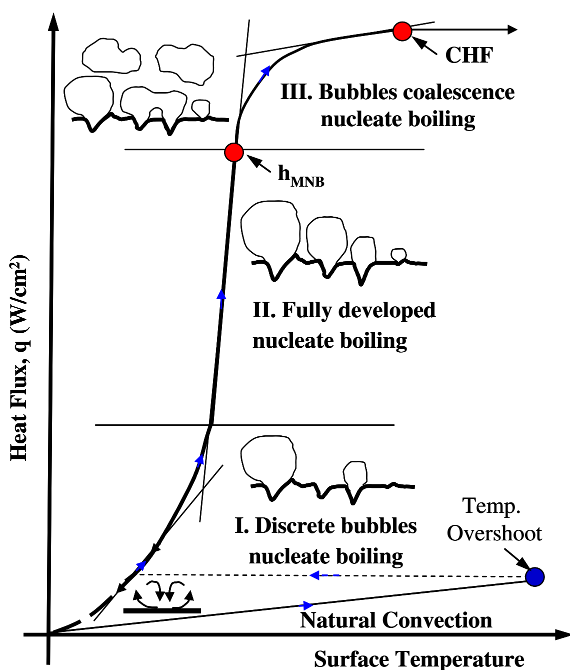

Fig. 1. A typical pool boiling curve of dielectric liquids.

$\Delta T_{sat} = (T_w - T_{sat})$, where T_{sat} is the liquid saturation temperature, are higher than at $h_{MNB.}$ For electronics cooling applications, it is preferable to operate near h_{MNB}, on the left side of the pool boiling curve, where the surface superheat is low (Fig. 1).

Enhancements in nucleate boiling of dielectric liquids on micro- and macro-structured or porous surfaces, surfaces with reentrant cavities, fabricated pores or micro-fins, roughened and micro-structured surfaces, surfaces with micro-porous coatings and metal foam have been reported. In addition to increasing CHF and the nucleate boiling heat transfer coefficient, excursions in the surface temperature before initiating nucleate boiling had either been eliminated or markedly reduced. Recently reported results of nucleate boiling enhancements on copper dendrites and micro-porous surfaces deposited using electrochemical processes (Fig. 2) have been very promising (El-Genk and Ali, 2010a,b; Kim, 2006; Furberg, 2006; Furberg et al., 2006; Shin et al., 2003). The micro-structure of these surfaces is relatively complex (Figs. 3–7). It consists of a repeated pattern of circular macro-pores surrounded by a relatively dense micro-structure of growing and branching copper dendrites (El-Genk and Ali, 2010a,b; Shin and Liu, 2004; Kim, 2006; Furberg, 2006). The Cu dendrites micro-structure is quite delicate and easily damaged, chipped and pealed off the cu substrate, compromising its potential for practical applications, unless it is strengthened, which is done in the present work.

On the other hands, thin metal dendrites and micro-porous layers (<400 μm thick) are easy and inexpensive to grow onto metal surfaces using electrochemical processes that are widely used commercially for electroplating and other similar applications. Compared to other methods in the literature of fabricating micro-structured, micro-finned and -porous surfaces and applying micro-porous coatings, electrochemical deposition employed in the present work is very simple, well controlled, and reproducible. It could also be used for depositing large surfaces of several to 10's of centimeters in length scale.

During electrochemical deposition, there are a number of controlled parameters that affect the thickness, micro-structure, volume porosity, and size and number of the macro-pores, the morphology and the structural strength of the deposited surface layers. These parameters include the deposition DC current density and time, the composition and concentration of the electrolyte solution, and the copper anode surface area and its separation distance from the copper cathode substrate. Very little work has been reported on pool boiling of dielectric liquids on metal dendrites/micro-porous surface layers (e.g., Kim et al., 2007; Li et al., 2008; El-Genk and Ali, 2010a,b; Albertson, 1977; Furberg, 2006; Furberg et al., 2006; Shin et al., 2003).

This paper extends the work recently published by El-Genk and Ali (2010b) on the enchantment of saturation boiling of PF-5060 dielectric liquid (3M, 2009b) on Cu micro-porous surface layers deposited using electrochemical processes on 10 × 10 mm and 1.38–1.6-mm thick Cu substrates. This paper extends the range of the surface layer thicknesses deposited and tested (95–220 μm) and experimentally investigates the effects of thickness, micro-structure and surface morphology on nucleate boiling heat transfer coefficient, CHF and eliminating or reducing the excursion in surface temperature prior to initiating boiling. Two-stage, electrochemical process is used to deposit the Cu micro-porous surface layers (Table 1) employed in the present pool boiling experiments. A basic dendrites micro-structure is deposited in the first stage using a high electrical current density of 3 A/cm^2 for 15–44 s, depending on the thickness. It is then structurally strengthened, for improved handling, by continuing electrochemical deposition at a much lower current density for 10's of minutes. The resulting micro-porous surface layers become strong enough as not to peel or chip off during subsequent fabrication of the test section and use in the boiling experiments.

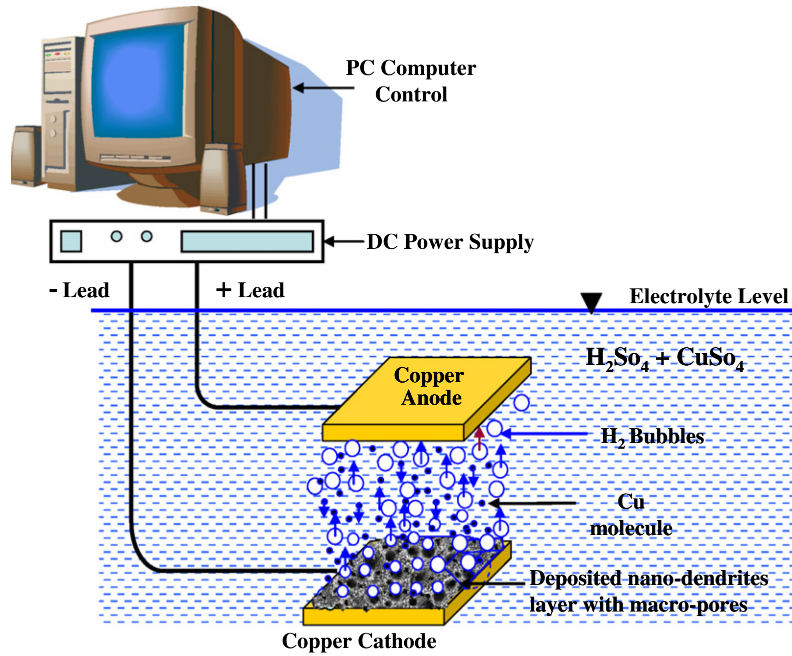

Fig. 2. Schematic of electrochemical deposition of the Cu micro-porous surface layers.

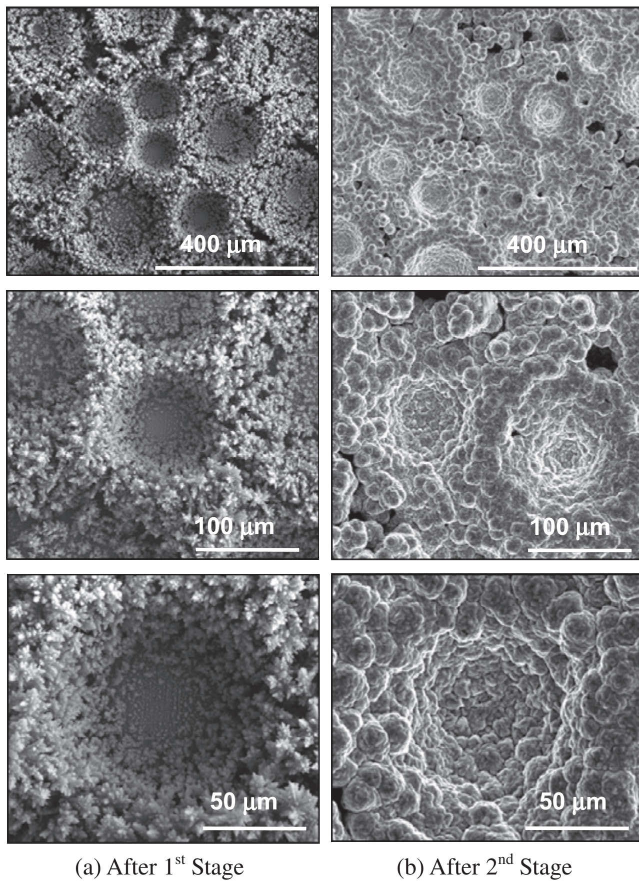

Fig. 3. SEM images of the Cu micro-porous surface layer #1 (95.1 ± 1.81 µm) at different magnifications.

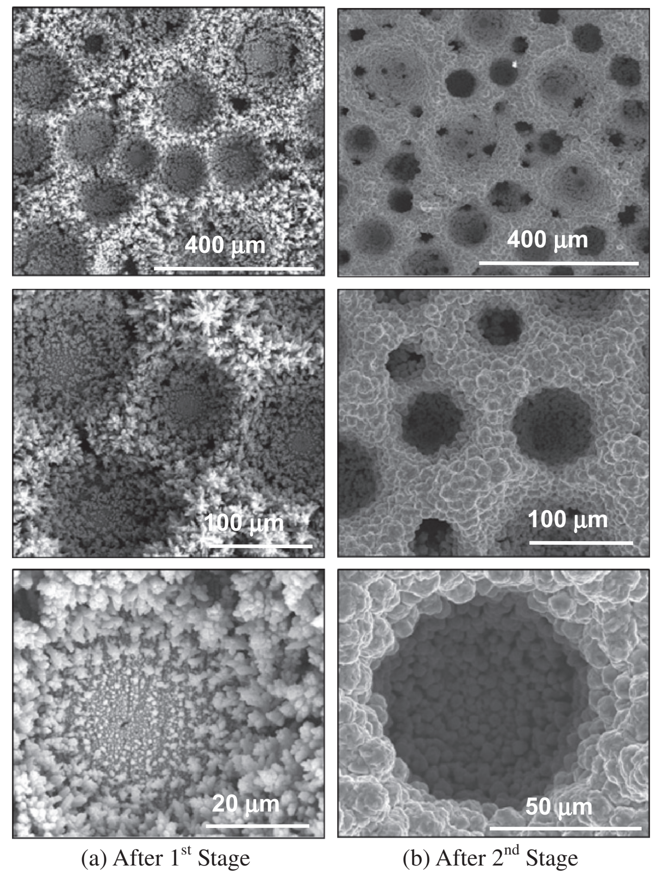

Fig. 4. SEM images of the Cu micro-porous surface layer #2 (139.4 ± 2.64 µm) at different magnifications.

1.1. Electrochemical deposition

The Cu micro-porous layers of the different thicknesses (Table 1) are deposited onto Cu substrates measuring 10 × 10 mm and 1.38–1.6 mm thick. The substrates function as the Cathode during the electrochemical deposition process and are laid out horizontal and parallel to a copper anode of larger surface area (4.5–5 cm^2). This ensures a uniform electrochemical deposition of Cu atoms

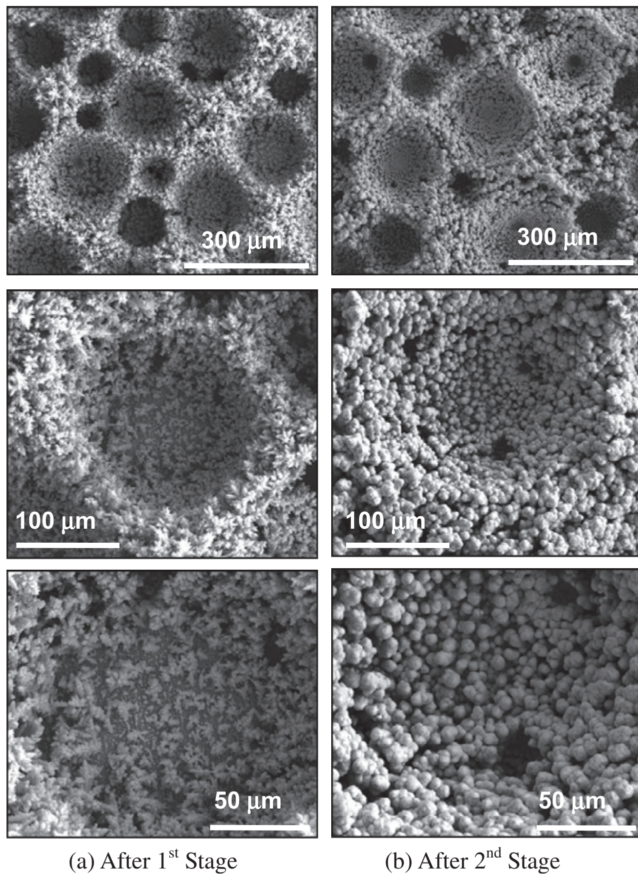

Fig. 5. SEM images of the Cu micro-porous surface layer #3 (171.1 ± 3.13 µm) at different magnifications.

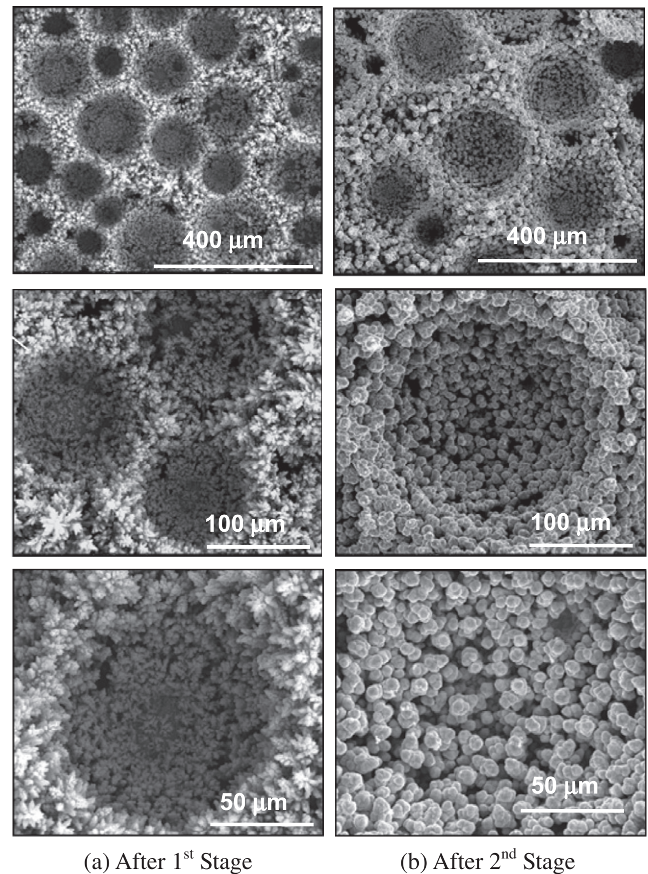

Fig. 6. SEM images of the Cu micro-porous surface layer #4 (197.4 ± 3.61 µm) at different magnifications.

onto the substrates. During the electrochemical deposition, the Cu cathode and the anode are fully immersed in the electrolyte solution of sulfuric acid and copper sulfate (Fig. 2 and Table 1) and separated by 2 cm. The cathode and the anode are connected to an external DC power supply, controlled by a PC, to adjust the supplied current density and monitor the disposition time (Fig. 2). When the electric current is supplied to the electrochemical deposition cell, the Cu^{+2} and H^{+} ions in the electrolyte solution undergo two simultaneous reduction reactions at the cathode:

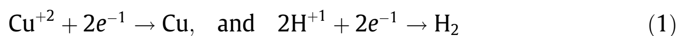

$$Cu^{+2} + 2e^{-1} \rightarrow Cu, \quad \text{and} \quad 2H^{+1} + 2e^{-1} \rightarrow H_2 \tag{1}$$

The electrochemical deposition of the copper micro-porous surface layers is carried out in two successive stages using the same electrolyte solution (Table 1).

The thickness and the basic dendrites micro-structure of the layers are established in the first stage using a current density of 3 A/cm^2 for 15–44 s, depending on the thickness (Table 1). During this stage, the deposited copper atoms on the cathode surface nucleate and grow rapidly in the form of fine and dense dendrites that surround open, circular macro-pores (Figs. 3a–7a). The hydrogen molecules evolving at the cathode form tiny bubbles that subsequently coalesce into dense streams of rising large bubbles. The columns of rising baubles are responsible for the formation of the patterned arrangement and the size of the openings of the macro-pores (Figs 3a–7a). The initially deposited micro-structures with volume porosities (>90%) and orderly arranged macro-pores are very delicate for handling, easily chipped and cracked.

To strengthen these micro-structures, electrochemical deposition continued at much lower current density for additional 10's of minutes. During this stage, the rate of deposition of the Cu atoms into the cathode is very low, negligibly changing the thickness of the Cu dendrite surface layer. The Cu atoms that partially fill out the dendrites structure and some of the macro-pores (Figs. 3b–7b) change the surface morphology and the volume porosity. The strengthened Cu surface layers become less porous (65–80 vol.%), but the wetted area of the surface increases due to the resulting micro-porous morphology and the formation of rounded depressions in the surface layers (Figs 3b–7b). The adhesion of the Cu micro-porous surface layers to the Cu substrates (Table 1) is very good for handing during the fabrication of the test section (Fig. 8) and the conduct of the pool boiling experiments. Preparation and cleaning of the Cu anode and Cu substrate (cathode) before starting the electrochemical deposition are critical for obtaining good adhesion and reproducibility of the micro-structure. More details on the two-stage electrochemical disposition process are given next.

1.2. First stage of deposition

During this stage of high current density (3 A/cm^2), the columns of rising hydrogen bubbles generating at the cathode surface form the circular macro-pores (Figs 3a–7a). These macro-pores are surrounded by a complex micro-structure of branching Cu dendrites that grow onto the cathode Cu substrate, surrounding patterned circular macro-pores. The continuous migration of copper and hydrogen ions, Cu^{+2} and H^{+} from the electrolyte solution to the cathode surface sustains the growth of the Cu dendrites, increasing the thickness of the deposited layer. Because the mobility of H^{+} ions is higher than that of Cu^{+2} ions, the former migrate to the cathode faster, increasing the number and generation rate of hydrogen

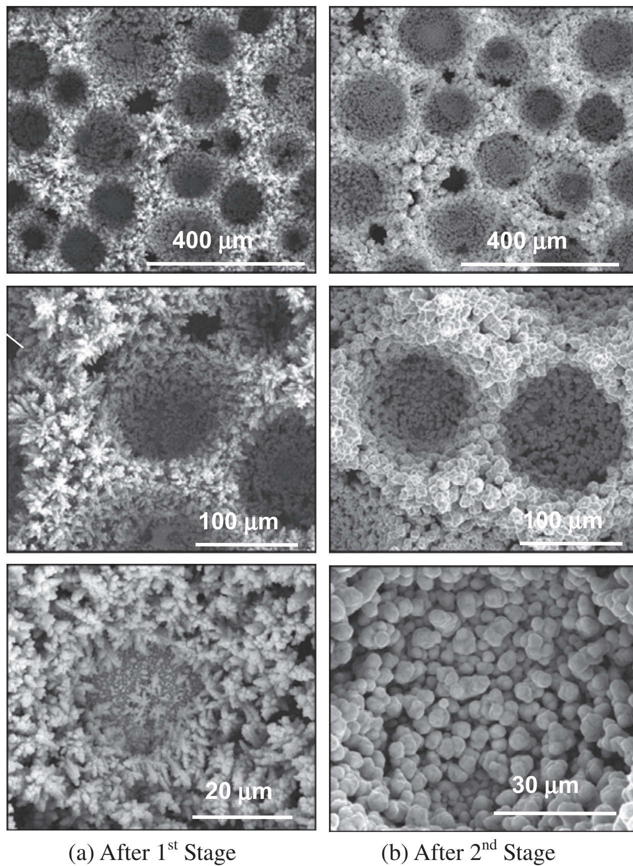

Fig. 7. SEM images of the Cu micro-porous surface layer #5 (230.3 ± 4.2 µm) at different magnifications.

bubbles. The initially deposited Cu nano-dendrites provide additional active reduction sites for incoming H^+ and Cu^{+2} ions, sustaining the generation of the hydrogen bubbles and the growth of the Cu nano-dendrites.

The rising columns of hydrogen bubbles increase the average opening of the macro-pores as the thickness of the deposited layer increases (Figs 3a–7a). The generation and rising of the hydrogen bubbles locally neutralize the cathode surface, producing the orderly patterned macro-pores, a few to 10's of micron in diameter (Figs. 3a–7a). On the other hand, the micro-pores within the Cu dendrites structure are very small, ranging in size from a fraction of micron to a few microns. SEM images of different magnifications of the deposited Cu dendrites layers during the first stage are presented in Figs. 3a–7a. They clearly show the macro-pores surrounded by the Cu dendrites. In addition to increasing the opening of the macro-pores, increasing the thickness of the deposited Cu dendrites layer slightly increases its volume porosity (Table 1). At the end of the first stage (Figs 3a–7a) the volume porosity ranges from 93.1% to 94.5%, almost independent of the thickness (Table 1). As indicated earlier, the deposited Cu dendrites structures during this stage are very delicate, easily chipped and cracked during subsequent fabrication of the test section (Fig. 8). To eliminate this shortcoming, electrochemical deposition continued beyond the first stage, but at a much lower current density for 10's of minutes, masking the fine Cu dendrites structure and forming a micro-porous surface.

1.3. Second stage of deposition

During this stage of very low current density for 10's of minutes (Table 1), the production of hydrogen bubbles ceases because of the low hydrogen atoms concentration at the cathode. Also, the deposition rate of Cu atoms onto the cathode is very low to

Table 1
Deposited and mechanically strengthened Cu micro-porous surfaces.

Layer #	Electrolyte (mol/l)	Current density (A/cm²)		Deposition time (s)		Est. thickness (µm)	Est. porosity (%)	
		1st	2nd	1st	2nd		1st	2nd
1	0.8 $CuSO_4$ + 1.5 H_2SO_4	3	V. low	15	100's	95.1 ± 1.81	94.5	65.3
2	0.8 $CuSO_4$ + 1.5 H_2SO_4	3	V. low	25	100's	139.4 ± 2.64	93.8	73.9
3	0.8 $CuSO_4$ + 1.5 H_2SO_4	3	V. low	30	100's	171.1 ± 3.13	93.7	76.8
4	0.8 $CuSO_4$ + 1.5 H_2SO_4	3	V. low	35	100's	197.4 ± 3.61	93.6	79.0
5	0.8 $CuSO_4$ + 1.5 H_2SO_4	3	V. low	44	100's	230.3 ± 4.2	93.1	80.6

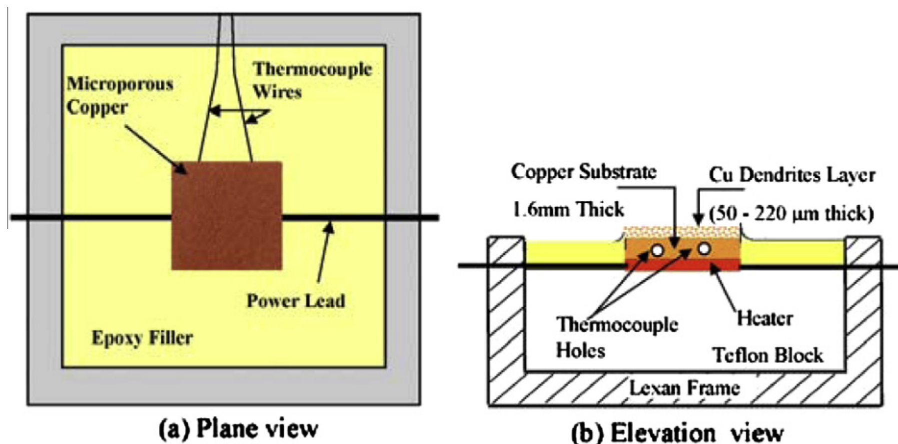

Fig. 8. Cross-sectional views of the assembled test section for the pool boiling experiments.

change the thickness, but it changes the surface morphology and reduces the volume porosity. The resulting micro-structure is rugged and excellent for handing in the boiling experiments. The strengthened micro-structure at the end of this stage of the electrochemical disposition process has lower volume porosity, but larger wetted surface area (Figs. 3b–7b). The average volume porosity of the Cu micro-porous surface layers decreases, but its value increases with increased thickness. It is estimated to be ~65.3% for surface layer #1 and as much as 80.6% for surface layer #5 (Table 1).

Figs. 3b–7b show SEM images at different magnifications of the structurally strengthened Cu micro-porous surface layers obtained at the end of the second stage and then used in the present pool boiling experiments. These images indicate that while the electrochemical deposition in the second stage strengthens the micro-structure, it masks the original dendrites (Figs. 3a–7a) by filling out the micropores in the dendrites and some of the originally open macro-pores with Cu atoms, clusters of atoms and micro-particles. The filled out macro-pores effectively increase the wetted surface area for nucleate boiling and are indicated by the large and deep hemi-spherical depressions in the SEM images in Figs. 3b–7b. They range in diameter from 30 to 60 μm, depending on the thickness of the deposited layer. The increased wetted surface area is expected to increase the number of active sites for bubbles nucleation and hence, the rates of nucleate boiling heat transfer in the pool boiling experiments. The combined effects of the surface morphology and increased wetted surface area would affect the potential for enhancing nucleate boiling heat transfer and increasing CHF, which are investigated next for saturation boiling of the PF-5060 dielectric liquid. It is worth noting the high wetting nature of the PF-5060 dielectric liquid, with a contact angle on Cu < 5°. The structurally strengthened Cu micro-porous surface layers (Table 1 and Figs. 3b–7b) are assembled into separate test sections for performing the pool boiling experiments. Several test sections for each type of the surface layers are constructed to demonstrate reproducibility of the electrochemical disposition process and of the nucleate boiling heat transfer results in the experiments.

2. Test section

The assembled test sections (Fig. 8) for the pool boiling experiments measure 30 mm × 30 mm in outside dimensions. Each consists of a Teflon block with a 1.0 mm deep square cavity (~10 × 10 mm) at the center of the top surface in which a high flux heating element and the Cu substrate, with the deposited Cu micro-porous layer, are placed. The 10 × 10 mm and copper substrate with the deposited Cu micro-porous surface layer is mounted on top of the heating element using thermally conductive epoxy (Fig. 8b). The copper substrate has two 0.6 mm diameter horizontal holes drilled on one side. They are equidistance from the top and bottom surfaces and penetrate half way into the Cu substrate (Fig. 8b). The measuring tips of the two K-type thermocouples are securely attached to the inside of the holes using a thermally conductive epoxy. The average reading of these thermocouples is taken as the average surface temperature for the purpose of constructing the pool boiling curves, after accounting for the temperature drop by conduction in the Cu substrate and the Cu microporous surface layer (⩽0.5 K).

The Teflon block of the test section is encased in a Lexan frame with closed bottom (Fig. 8b). The shallow cavity on top of the Teflon block, which surrounds the mounted Cu substrate with the deposited surface layer, is filled with translucent epoxy adhesive; flush with the micro-porous Cu surface. The purpose is to strengthen the mounted substrate and prevent the formation of micro-cracks at the edges that would cause bubbles to nucleate and skew the pool boiling curve (Fig. 8a). The setup and procedures for conducting the boiling experiments are briefly described next.

3. Experimental setup and procedures

The test facility for conducting the boiling experiments has been described in details elsewhere (El-Genk and Parker, 2008; Parker and El-Genk, 2005, 2006; El-Genk and Bostanci, 2003, El-Genk and Ali, 2010b) and only briefly summarized herein. It consists of a polycarbonate hot water bath with electrical heater for minimizing the side heat losses from the test vessel immersed in it and for maintaining the temperature of the PF-5060 liquid pool in the test vessel constant.

The test vessel has a tightly sealed cover to minimize loss of the volatile PF-5060 dielectric liquid, thus maintaining a constant liquid level above the test section (~8 cm) in the experiments. The hot water bath and the two submerged cooling coils in the liquid pool in the test vessel maintain the temperature of the PF-5060 dielectric liquid constant within ± 0.5 K of its saturation temperature (51.4 °C at the ambient pressure in Albuquerque, NM, located ~1.5 km above sea level). The water-cooled copper coil located below the cover plate of the test vessel condenses the vapor generated by the test section in the experiments.

The magnetic stirrer at the bottom of the test vessel speeds up the out-gassing of the PF-5060 liquid and ensures a uniform pool temperature prior to conducting the experiments. Because of the high air solubility in PF-5060, it takes typically more than 2 h to outgas the liquid pool in the test vessel. The liquid pool temperature is monitored using four K-type thermocouples placed at different locations. The pool temperature is taken as the average reading of the two thermocouples placed in the copper substrate near the boiling surface (Fig. 8b).

The heat losses through the sides, top and bottom of the assembled test section (Fig. 8) are calculated using the ANSYS finite element commercial software to be negligibly small (El-Genk and Parker, 2008; Parker and El-Genk, 2005, 2006; El-Genk and Bostanci, 2003). Thus, the dissipated power from the uniformly heated, 10 × 10 mm Cu micro-porous surface layer is assumed to equal that generated by the underlying heating element in the test section. This power, determined from the measured voltage across and the electric current provided to the heating element by a DC power supply is that dissipated from the exposed surface of the Cu micro-porous layer for the purpose of constructing the pool boiling curve.

In the boiling experiments, the electrical power supplied to the heating element in the test section is increased slowly by incrementally raising the applied voltage by <0.02 V at a time. The size of the voltage increment is decreased gradually as the boiling curve approaches CHF in order to limit the temperature overshot associated with CHF and avoid burning the heating element. Following each incremental increase in the applied voltage, the surface heat flux and the average surface temperature, after accounting for the temperature drop due to conduction in the Cu substrate to the boiling surface (<0.5 K), are recorded only after reaching steady state. This is when the difference between two successive measurements of the average surface temperature is within ±0.2 K. Each of these surface temperatures is the average of 30 readings of each of the two thermocouples embedded in the Cu substrate (Fig. 8b). When either of these thermocouples detects a temperature increase in excess of 30 K in two consecutive steady state measurements, it is considered an indication of reaching CHF, and the experiment is terminated. This procedure protects the heating element in the test section from burning out when reaching CHF.

The estimated uncertainties in the present boiling experiments are ±0.2 K and ±0.10 mV in the temperature and applied voltage measurements, ±2.2% and ±3.9% in nucleate boiling heat flux and heat transfer coefficient,±2.3% in the CHF determined using the procedure described earlier, and 1–3 K in surface temperature at CHF. These uncertainties are based on the methodology outlined by Kline (1985).

4. Experimental results

Pool boiling experiments are conducted to investigate potential enhancements in saturation nucleate boiling of PF-5060 dielectric liquid on structurally strengthened, Cu micro-porous surface layers (Table 1 and Figs. 3b–7b). The experiments investigated the effects of the thickness and the surface morphology of these layers on CHF and nucleate boiling heat transfer coefficient, h_{NB}, and the corresponding surface superheats and on eliminating or reducing the excursion in surface temperature prior to the nucleate boiling incipience (Figs. 9–13). The structurally strengthened surface layers (Figs. 3b–7b) are used individually in the saturation pool boiling experiments and the obtained pool boiling curves and those of the nucleate boiling heat transfer coefficient are presented in Figs. 9–13.

The results for PF-5060 dielectric liquid on surface layers #2 and #3 (Table 1 and Figs. 4b and 5b) are compared to those reported by others for saturation boiling of both FC-72 and PF-5060 on plane, micro-porous and micro- and nano-structured and micro-finned surfaces (Parker and El-Genk, 2005; Kim, 2006; Wei and Honda, 2003; Ghiu, 2007; Sriraman and Banerjee, 2007). PF-5060 is relatively less expensive and has the same physical properties and saturation temperature as FC-72, except that its surface tension is ~20% higher (3M, 2009a,b; El-Genk and Ali, 2010b).

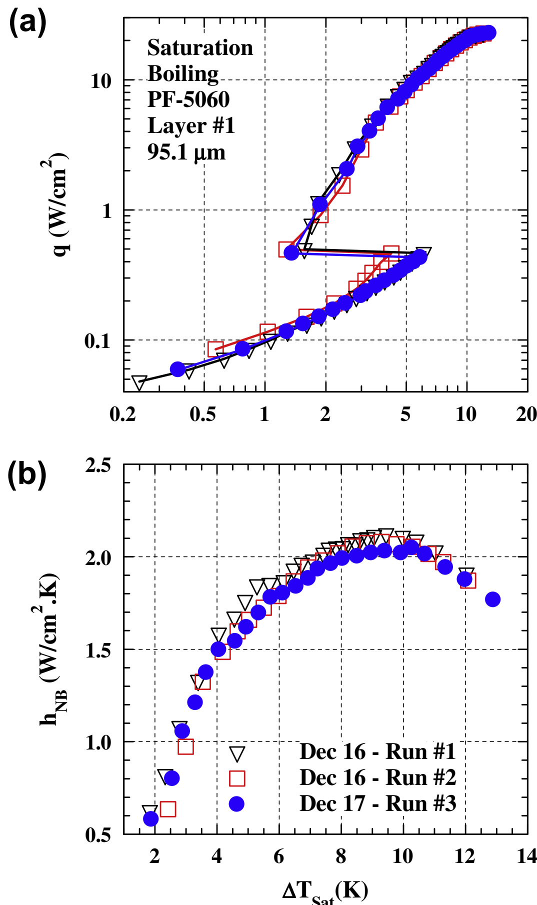

Fig. 9. Saturation pool boiling and h_{NB} curves for PF-5060 on surface layer #1.

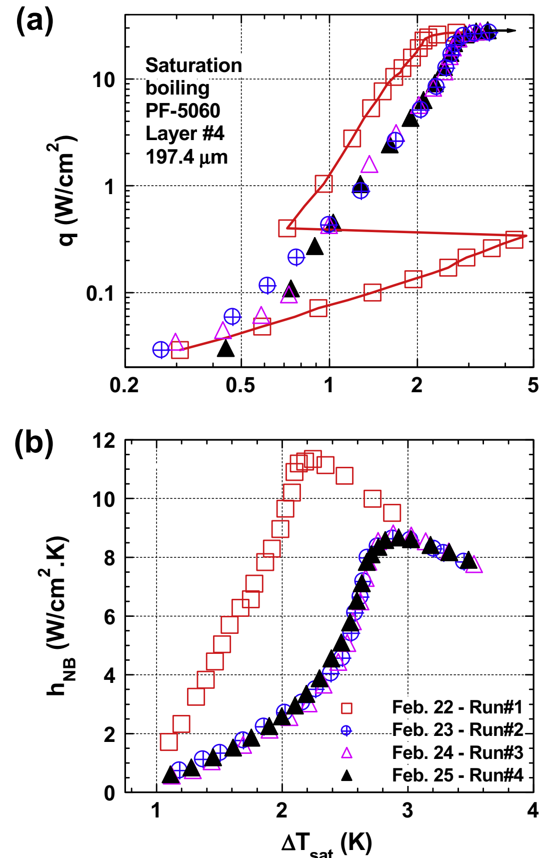

Fig. 10. Saturation pool boiling and h_{NB} curves for PF-5060 on surface layer #4.

4.1. Conditioning the surface layers

The saturation pool boiling and the nucleate boiling heat transfer coefficient curves of PF-5060 liquid on the structurally strengthened layers #1 and #4 (Table 1 and Figs. 3b and 6b) are presented in Figs. 9 and 10. The best nucleate boiling curves are typically when the Cu micro-porous surface layers (Table 1) are used for the first time (Figs. 9–13). However, for these surfaces the excursion in surface temperature prior of initiating nucleate boiling is also the highest, but much smaller than those reported in the literature for plane Cu and silicon surfaces (Rainey and You, 2000; Parker and El-Genk, 2005; El-Genk and Bostanci, 2003; Chang et al., 1998). Surface conditioning is typically associated with a gradual decrease in the nucleate boiling heat flux, q, and a shift of the pool boiling curves to higher surface superheats. This decreases the nucleate boiling heat transfer coefficient, but not necessarily CHF. For the conditioned surface layers, the pool boiling curves are highly reproducible with no or very little shift to higher surface superheats. Surface conditioning is achieved after conducting several pool boiling experiments, each lasting typically 4–5 h, separated by cool down intervals of 2–14 h (solid symbols in Figs. 9–13).

These figures clearly show that the saturation pool boiling curves of PF-5060 on the structurally strengthened (Table 1) and conditioned (Figs. 3b–7b) Cu micro-porous surfaces in the last two boiling tests are almost identical. The values of CHF, indicated by the last data points on the boiling curves in Figs. 9–13, and the corresponding surface superheats strongly depend on the

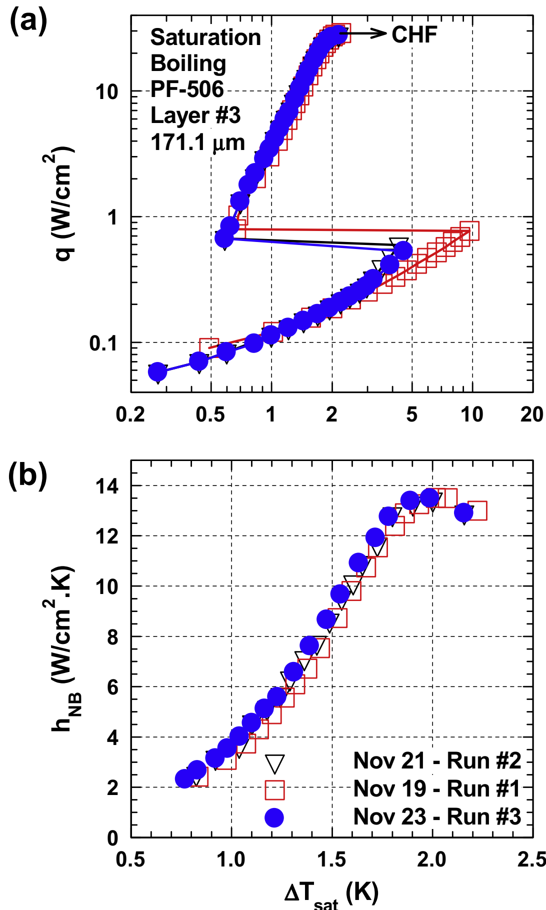

Fig. 11. Saturation pool boiling and h_{NB} curves for PF-5060 on surface layer #3.

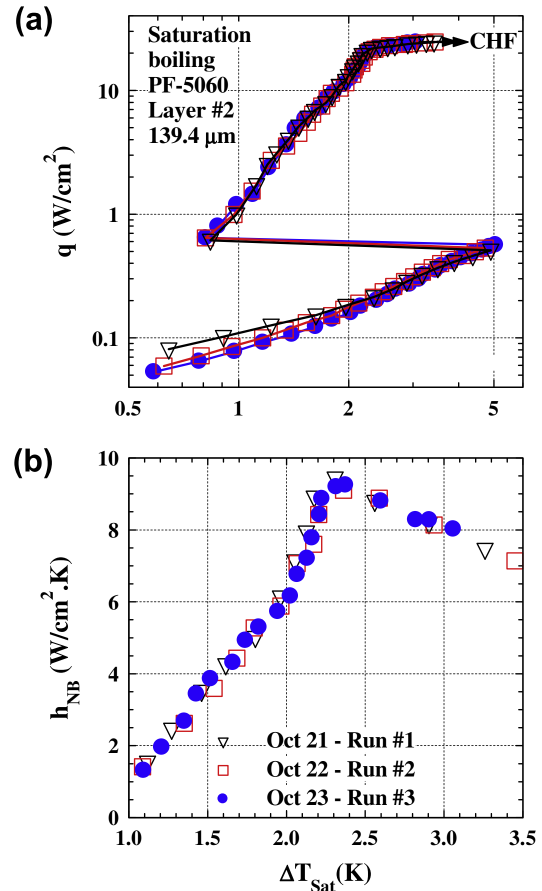

Fig. 12. Saturation pool boiling and h_{NB} curves for PF-5060 on surface layer #2.

thickness and the morphology of the surface layers. The saturation pool boiling and nucleate boiling heat transfer coefficient curves for PF-5060 on surface layer #1, of the smallest thickness (Fig. 9 and Table 1), show that surface conditioning is achieved after three consecutive boiling tests. The boiling heat transfer results on the conditioned surface layer #1 are those given by the solid circle symbols in Fig. 9a and b.

Fig. 9a shows that the measured excursion in the surface temperature prior to initiating nucleate boiling on this surface layer is <7 K, and did not decrease for the conditioned surface after three consecutive boiling tests. The saturation CHF of PF-5060 on the conditioned surface layer #1 is 22.76 W/cm^2 and occurs at a surface superheat, ΔT_{sat} = 12.89 K (Fig. 9a). The maximum nucleate boiling heat transfer coefficient, h_{MNB}, near the end of the fully-developed nucleate boiling region II (Fig. 1) is 2.05 W/cm^2 K and occurs at ΔT_{sat} = 10.27 K (Fig. 9b).

The saturation pool boiling curves for the surface layer #4 (197.4-μm thick) are given in Fig. 10a and b. The saturation CHF of PF-5060 on the conditioned surface layer #4 (Fig. 10a) is ~27.36 W/cm^2 and 27.83 W/cm^2 for surface layer #3 (Fig. 11a). For the conditioned surface layers #2 and #5, CHF is 24.54 and 27.43 W/cm^2, respectively, (Figs. 12a and 13a). On plane copper and silicon surfaces, the saturation boiling CHF for FC-72 and PF-5060 ranges from 13 to 16 W/cm^2, depending on the surface roughness (e.g., Rainey and You, 2000; Parker and El-Genk, 2005; El-Genk and Bostanci, 2003; Chang et al., 1998). The saturation CHF value for PF-5060 is the highest on the surface layer #3 (Figs. 14a) and the corresponding surface superheat of 2.16 K is the lowest. This temperature superheat increases precipitously with either increasing or decreasing the thickness of the surface layer (Fig. 14a). Fig. 14b shows that h_{MNB} initially increases with increased thickness of the structurally strengthened and conditioned micro-porous surface layers, peaks on surface layer #3, then decreases with increased layer thickness. Its lowest value is on surface #1 (2.05 W/cm^2 K), followed by that on surface layer #5 (7.53 W/cm^2 K). The corresponding surface superheat decreases slightly to its lowest value on surface layers #3 (2.0 K) then increases with a further increase or decrease in the thickness of the surface layer (Fig. 14b).

The present saturation pool boiling curves for PF-5060 (Figs. 9a–13a) show that nucleate boiling heat flux progressively increases with increased surface superheat until reaching CHF. However, the nucleate boiling heat transfer coefficient initially increases with increased surface superheat to a maximum, h_{MNB}, near the end of the fully-developed nucleate boiling region II (Fig. 1). It then decreases with further increase in the surface superheat until reaching CHF (Figs. 9b–13b) because of the added heat transfer resistance due to the coalescence of the growing and rising bubbles at and near the surface. Thus, h_{MNB} is much higher than at CHF and the corresponding surface superheat is lower (Figs. 9b and 13b).

For saturation boiling of PF-5060 on the structurally strengthened and conditioned surface layer #3 (Table 1 and Fig. 5b), h_{MNB} = 13.5 W/cm^2 K and occurs at ΔT_{sat} of only 2.0 K, compared to 12.9 W/cm^2 K and 2.16 K at CHF (Fig. 11). Similarly, on the surface layers #1, #2, #4 and #5 (Figs. 3b, 4b, 6b and 7b), h_{MNB} = 2.05, 9.25, 8.6 and 7.53 W/cm^2 K and occurs at ΔT_{sat} = 10.27, 2.37, 2.93 and 2.88 K, respectively (Figs. 9b, 10b, 12b and 13b). For these layers, the nucleate boiling heat transfer coefficient at CHF is 1.766, 8.02, 7.86, and 5.51 W/cm^2 K and the corresponding surface superheat is 12.9, 3.06, 3.48 and 5 K, respectively. These results confirms

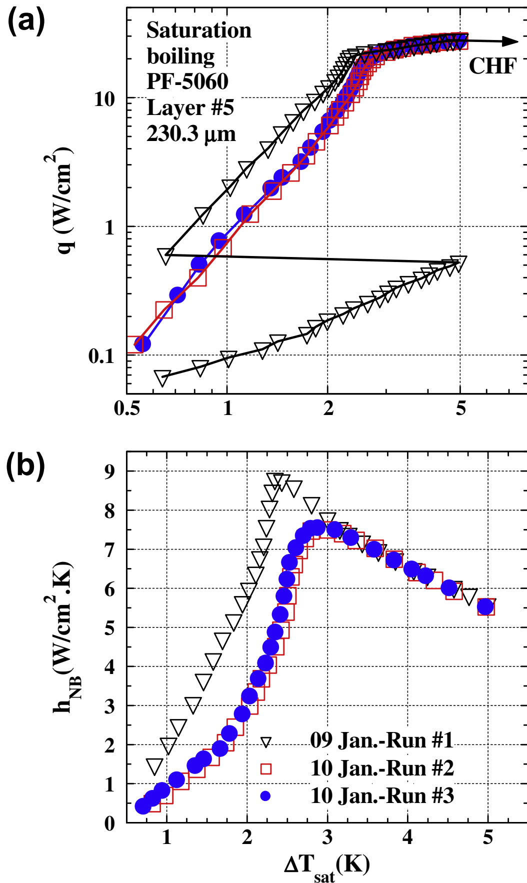

Fig. 13. Saturation pool boiling and h_{NB} curves for PF-5060 on surface layer #5.

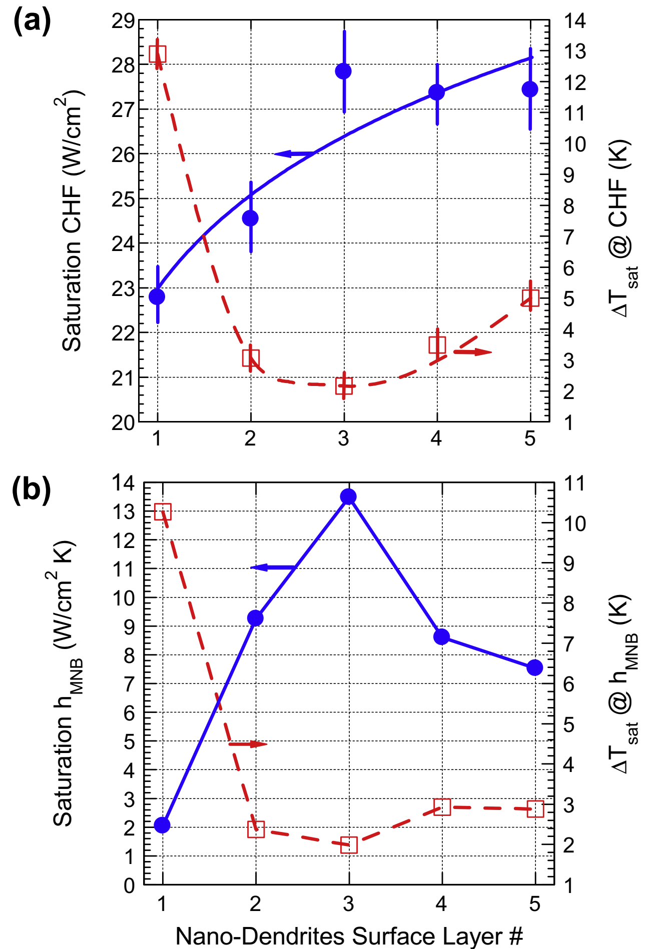

Fig. 14. Comparison of saturation CHF and h_{MNB} and corresponding surface superheats for different layers.

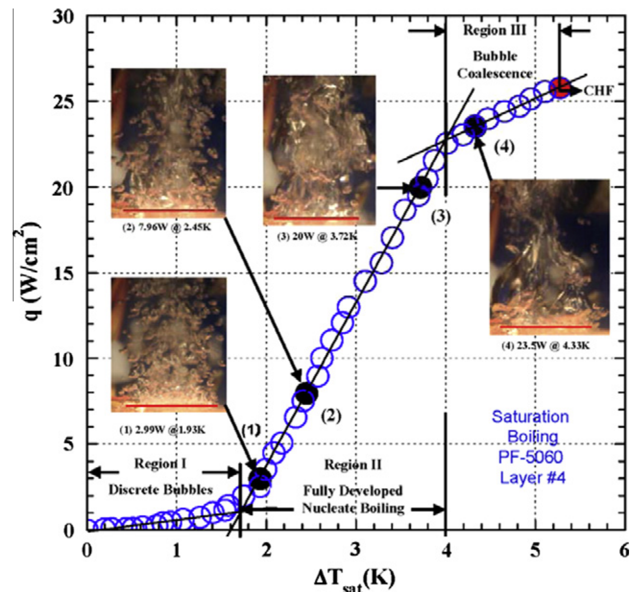

Fig. 15. Saturation boiling curve for PF-5060 on the Cu micro-porous surface layer #4 with photographs.

that the Cu micro-porous surface layers #2 to #5 significantly enhance nucleate boiling of PF-5060, with h_{MNB} values of 7.53–13.5 W/cm^2 K occurring at surface superheats of only 2.0–2.88 K.

The highest h_{MNB} is by far that on the surface layer #3 (13.5 W/cm^2 K), followed by that on the surface layer #2 of 9.25 W/cm^2 K (Table 1 and Figs. 11b and 12b). The h_{MNB} of PF-5060 on the thinnest surface layer #1 (Fig. 9b) is the lowest (2.05 W/cm^2 K), but it is more than twice that of FC-72 on a plane copper surface (<0.8 W/cm^2 K) (e.g., Rainey and You, 2000; Parker and El-Genk, 2005; Chang et al., 1998). The present results also show that a temperature excursion prior to initiating nucleate boiling typically occurs when the surface layers are used for the first time, but it is generally much lower (<10 K) than those reported for pool boiling on plane copper and silicon surfaces (15–25 K) (Parker and El-Genk, 2005; Vemuri and Kim, 2005). For saturation boiling of PF-5060 on the conditioned Cu micro-porous surface layers in Table 1, the temperature excursion prior to initiating nucleate boiling is either decreased (<7 K) or eliminated (Figs. 9a–13a).

Fig. 15 presents the saturation pool boiling curves of PF-5060 on the structurally strengthened and conditioned surface layer #4 (Table 1 and Fig. 6b), with inserted photographs of the boiling process in the different regions. Note that for this surface, nucleate boiling started at a surface superheat <0.5 K, and hence there is no excursion in the surface temperature prior to initiating nucleate boiling (Fig. 10a).

4.2. Boiling hysteresis

Boiling hysteresis is typically caused by the contributions of the thermal inertial of the surface and the metal substrate and the potential changes in the boiling process at the surface, when gradually increasing or decreasing the input power to the heating element in the test section. To examine the boiling hysteresis in the present experiments, identical tests are conducted using the

same surface layer. The obtained saturation boiling and nucleate boiling heat transfer coefficient curves of PF-5060 dielectric liquid on the conditioned surface layer #2 (Table 1 and Fig. 4b) are presented in Fig. 16a and b.

To quantify the boiling hysteresis in the present experiments, the pool boiling curves recorded in separate tests with ascending (or increasing heat flux) and descending (or decreasing heat flux) input power to the heating element in test section are compared (e.g., Fig. 16a). In the former, the input power to the heating element (Fig. 8b) increases incrementally as described earlier in the section on the experiments setup and procedures (solid circle symbols in Fig. 16a and b), until reaching CHF). In the other test, the pool boiling experiment starts at a high heat flux but below CHF (~20 W/cm^2) and the power supply to the heating element in the text section is decreased incrementally (open circle symbols in Fig. 16a and b).

The results in these figures for the surface layer #2 (Fig. 4b) clearly show that the nucleate boiling heat flux and the heat transfer coefficient curves obtained by incrementally increasing and decreasing the input power to the test section in the experiments are almost identical, thus, indicating little or no boiling hysteresis. These results suggest that the effect of the thermal inertia of the Cu dendrites and micro-porous surface layer and of the Cu substrates is small to cause notable hysteresis in the pool boiling curves in the experiments.

4.3. Effect of surface morphology and micro-structure

Figs. 9–13 present the obtained saturation pool boiling and the nucleate boiling heat transfer coefficient curves for PF-5060 dielectric liquid on the surface layers #1 to #5 (Table 1 and Figs. 3b–7b). These curves are also compared in Fig. 17a and b. In these figures, the last data points in the pool boiling and nucleate boiling heat transfer coefficient curves indicate CHF (closed circle symbols), determined following the procedures described earlier. The obtained values of the h_{MNB} for PF-5060 liquid on the different surface layers (Table 1) are also indicated in Fig. 17b (solid triangle symbols).

On all five Cu micro-porous surfaces investigated (Table 1 and Figs. 3b–7b), saturation CHF values of PF-5060 dielectric liquid ranges from 22.76 to 27.83 W/cm^2 and the corresponding surface superheat, ΔT_{sat}, ranges from as little as 2.16 K to 12.89 K. CHF on surface layer #2 is the highest (27.83 W/cm^2) and occurs at ΔT_{sat} of only 2.16 K. On surface layer #2, saturation CHF of PF-5060 is 24.5 W/cm^2 and occurs at ΔT_{sat} of 3.0. The saturation CHF of PF-5060 on surface layers #1, #4, and #5 are 22.78, 27.36 and 27.43 W/cm^2 and occur at ΔT_{sat} of 12.89, 3.48 and 5 K, respectively.

The present CHF values are considerably higher and the corresponding values of ΔT_{sat} are much lower than those reported for saturation boiling of either PF-5060 or FC-72 dielectric liquids by other investigators on plane copper and silicon surfaces (<16 W/cm^2) (e.g., Parker and El-Genk, 2005). The present CHF values are either higher or comparable to those reported for these dielectric liquids on micro-structured and micro-finned surfaces, micro-porous graphite and micro-porous coating (e.g., Kim et al., 2007, 2008; Chih et al., 2007; El-Genk and Parker, 2008; Rainey and You, 2000; Parker and El-Genk, 2005,2009; Vemuri and Kim, 2005; El-Genk and Bostanci, 2003; Launay et al., 2006; Kim, 2006; Wei and Honda, 2003; Ghiu, 2007; Sriraman and Banerjee, 2007; Chang and You, 1996; Jiang et al., 2001; Rajalu et al., 2004; Ramaswamy et al., 2003; Yu and Lu, 2007). For these surfaces, however, CHF

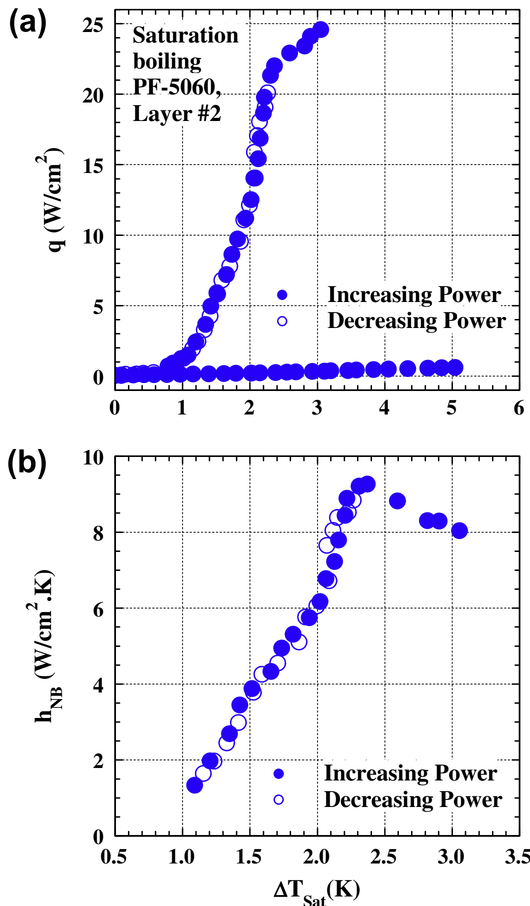

Fig. 16. Saturation boiling hysteresis of PF-5060 on the Cu micro-porous surface layer #2.

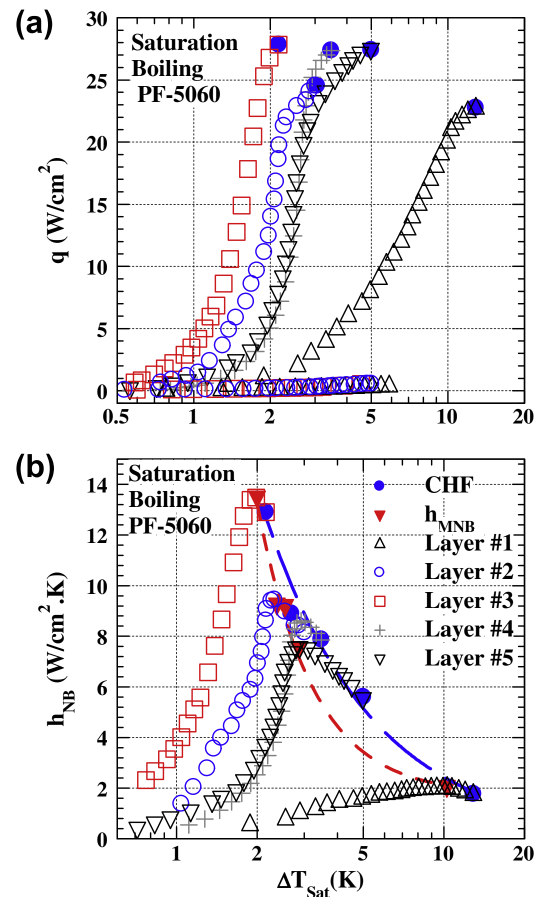

Fig. 17. Comparison of saturation boiling and h_{NB} curves of PF-5060 on the Cu micro-porous surface layers.

occurs at much higher surface superheats of 9–32 K, compared to <13 K in the present experiments (Figs. 17a and 18a). The present values of ΔT_{sat} at CHF correspond to surface temperatures of 53.5–64.4 K, which are significantly lower than recommended for the chip junctions' by the industry (<85 °C).

As shown in Fig. 17b, the highest nucleate boiling heat transfer coefficient is that on the structurally strengthened and conditioned surface layer #3, followed by layer #2, #4, and #5, respectively. For surface layer #3, h_{MNB} = 13.5 W/cm^2 K and occurs at ΔT_{sat} of only 2.0 K, compared to 2.05, 9.25, 8.6 and 7.53 W/cm^2 K on surface layers #1, #2, #4 and #5, respectively For these layers, the corresponding values of ΔT_{sat} are 10.27, 2.37 K, 2.93 K and 2.88 K, respectively (Fig. 17b).

4.4. Comparison with published work

Fig. 18 compares the present saturation boiling curve of PF-5060 dielectric liquid on the structurally strengthened and conditioned surface layers #2 and #3 (Table 1 and Figs. 11b and 12b) with those reported for FC-72 on a Cu dendrites surface by Kim (2006), on silicon with micro-pin fins by Wei and Honda (2003) and on micro-porous graphite and plane copper by Parker and El-Genk (2005), and for PF-5060 on silicon with Carbon nano-tubes (CNTs)-based pin fin arrays by Launay et al. (2006), on macro-structured surfaces by Ghiu (2007) and on nano-structured surfaces by Sriraman and Banerjee (2007). In this Figure, MAS stands for a macro-structured surface, MFS stands for a micro-finned surface, MPC stands for a macro-porous coating, MPG stands for micro-porous graphite, MIS stands for a micro-structured surface and NS stands for a nano-structured surface.

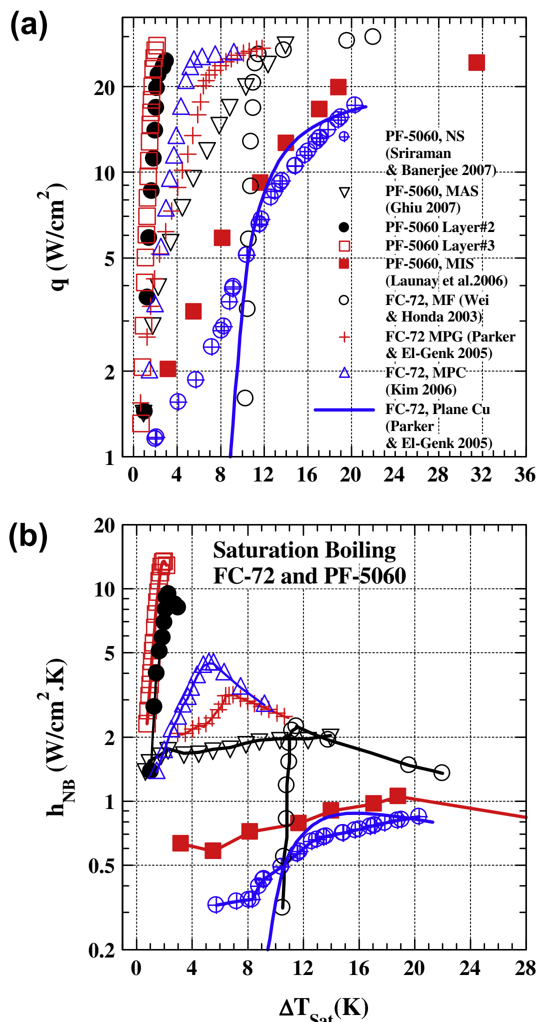

Fig. 18. Comparison of saturation boiling and h_{NB} curves on the Cu micro-porous surface layers #2 and #3 with those reported by other investigators for FC-72 and PF-5060.

The results delineated in Fig. 18 indicate that the saturation CHF value of Wei and Honda (2003) for FC-72 (29.8 W/cm^2) is the highest and that for FC-72 on plane copper of 17 W/cm^2 is the lowest (Parker and El-Genk, 2005). The present saturation CHF of PF-5060 on the Cu micro-porous layer #3 (Table 1) of 27.83 W/cm^2 occurs at the lowest surface superheat, ΔT_{sat} = 2.16 K. The reported CHF value by Kim (2006) for FC-72 on a Cu dendrites surface layer is comparable to the present value for PF-5060 on surface layer #2 (24.54 W/cm^2), but occurs at a much higher surface superheat (~9.5 K versus 3.0 K on surface layer #2) (Fig. 18a). On the other surfaces, the saturation boiling CHF values of both FC-72 and PF-5060 are not only lower but occur at higher surface superheats.

The present values of h_{MNB} for saturation boiling of PF-5060 on the structurally strengthened and conditioned surface layers #2 and #3 (Table 1 and Fig. 18b) of ~9.25 and 13.5 W/cm^2 K, respectively, are significantly higher than that of Kim (2006) for saturation FC-72 on a similar surface (~4.5 W/cm^2 K). They also occur at very low surface superheats of only 2.4 K and 2.0 K, respectively, versus ~5.5 K by Kim (2006) The present values of h_{MNB} for PF-5060 on surface layers #4 and #5 are 8.6 and 7.53 W/cm^2 K and occur at surface superheats of 2.93 K and 2.88 K, respectively (Fig. 17b). The reported h_{MNB} for saturation boiling of FC-72 on micro-porous graphite (Parker and El-Genk, 2005) is 3.2 W/cm^2 K and occurs at a surface superheat of 6.9 K (Fig. 18b). All the other h_{MNB} values for FC-72 and PF-5060 in Fig. 18a are much higher than those reported for saturation boiling of FC-72 on plane copper (0.8 W/cm^2 K) and occur at much higher surface superheats than for saturation PF-5060 on the present Cu dendrites and micro-porous surface layers (Table 1).

5. Discussion

The basic micro-structure, with patterned open macro-pores surrounded by fine and dense Cu dendrites, forms during the high current density (3 A/cm^2) electrochemical deposition stage, lasting 15–44 s, depending on the thickness. During this stage of deposition, the formation of dense columns of rising hydrogen bubbles at the cathode is responsible for the formation of the patterned macro-pores within the Cu dendrites micro-structure (Figs. 3a–7a and 19). Fig. 19 presents high magnification SEM images of the Cu dendrites and micro-porous surface layers #3 and #4 at the end of the 1st and 2nd stages of electrochemical deposition, respectively. The thicker the deposited layer the larger the macro-pores and the denser the surrounding Cu dendrites at the end of the first stage. The deposited micro-structure at the end of the first stage is highly porous (volume porosity > 90%), but fragile and delicate to handle during the assembly of the test section and the conduct of the boiling experiments.

Strengthening the micro-structure of the deposited Cu dendrites surface layers in the first stage is accomplished by continuing the electrochemical disposition process at a much lower current density for 10's of minutes with the same electrolyte solution. In this stage, the very low rate of disposition of the Cu atoms strengthens the micro-structure by filling up the Cu dendrites and some of the open macro-pores, insignificantly changes the thickness and surface morphology. The resulting Cu micro-porous structure forming at the end of the second has lower volume porosity and increases the wetted surface area. Such increase in the wetted surface area and the induced changes in the surface morphology together with the remaining open macro-pores might have

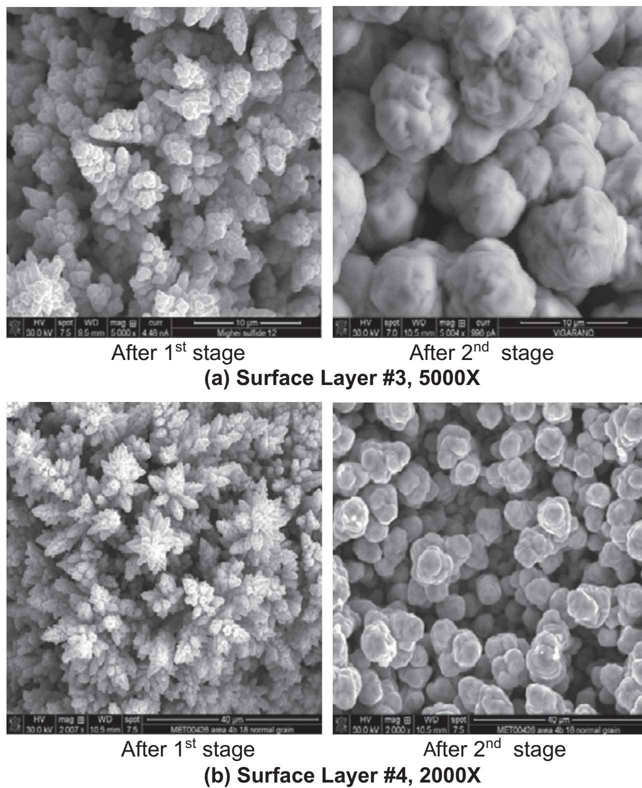

Fig. 19. SEM images of layers #3 and #4 at high magnifications showing the Cu dendrites structure forming at end of 1st stage and the Cu micro-porous surface resulting at the end of 2nd stage of electrochemical deposition.

contributed to the measured enhancements in saturation nucleate boiling of PF-5060 dielectric liquid in the present work. The Cu micro-porous surface layers (Table 1 and Figs. 3b–7b) have good adhesion to the Cu substrates and handle well during the assembly of the test sections and in the conduct of the pool boiling experiments.

The obtained pool boiling results on the structurally strengthened and conditioned Cu micro-porous surface layers (Table 1 and Figs. 3b–7b) show marked enhances in the saturation nucleate boiling heat transfer coefficient and increases in CHF at lower surface superheats. To the best of the authors' knowledge, the present values of the maximum nucleate boiling heat transfer coefficient, particularly those on surface layers #2 and #3, are significantly higher than has been reported in the literature for saturation boiling of either FC-72 or PF-5060 dielectric liquids on plane and macro- and micro-structured and micro-finned surfaces, macro-porous graphite, metal foams, and surfaces with micro-porous coatings.

The open pores in the structurally strengthened Cu micro-porous layers could have increased the liquid circulation from the overlaying pool through the heated surface layers by the capillary suction developing at the liquid–vapor interface in the capillaries within the micro-structure. The average size of these capillaries could range from a fraction of a micron to a few microns (Figs. 3–7). The developing capillary pressure is proportional to the surface tension of the PF-5060 dielectric liquid and inversely proportional to the average size of these capillaries. The liquid evaporation from the menisci at the interface between the liquid-feed capillaries and the vertical open macro-pores increases the vapor pressure in the macro-pores and form growing bubbles at the exposed surface. When the size of these bubbles is large enough for the buoyant force to overcome that due to surface tension at the opening of the macro-pores, they detach and other bubbles begin to grow at the same open macro-pores.

The recorded enhancements in both saturation CHF and nucleate boiling heat transfer coefficient in the present work could partially be attributed to the combined effects of the morphology and the relatively high volume porosity of the Cu micro-porous surface layers (Table 1 and Figs. 3b–7b). The increased wetted surface area due to the formation of semi-spherical depressions in the surface layers and the formation of micro-sized Cu particles on the surface during the second stage of disposition could both have increased the numbers and the density of the active sites for bubbles nucleation. A secondary effect could have been the decrease in lateral coalescence among growing and rising bubbles at and near the surface, which may explain the high CHF values.

The fact that dielectric liquids, including the PF-5060 used in the present pool boiling experiments, are highly wetting (very low surface tension) – a wetting angle for these liquids on plain copper is <5°, suggest that wetting was not an issue. The measured enhancements in nucleate boiling heat transfer could be attributed to a combination of increased wetted surface area and high active nucleation sites density for the deposited Cu micro-porous layers. Although the latter was not measured, the effect could be deduced from the obtained results showing high nucleate boiling heat transfer coefficient at low surface superheats (<7 K). The enhanced performance of surface layer #3 (the highest maximum nuclear boiling heat transfer coefficient and the lowest value of the corresponding surface superheat) could also be attributed to an increase in the density of the active nucleation sites on that surface, compared to the others.

Results also suggest that for both the thicker and thinner Cu micro-porous surface layers there might not have been enough entrapped air in some of the surface micro-pores to initiate the bubbles nucleation at the same intensity as the other surfaces. This is a strong possibility given the high wetting property of the PF-5060 dielectric liquid. On the other hand, the results in Fig. 14a clearly indicate that CHF increases monotonically with increased thickness of the deposited surface layer, but the corresponding surface superheat for surface layer #3 is the lowest. This again strengthens the notion that the high density of the active nucleation sites for vapor bubbles on that surface could have been directly responsible for the lower surface temperature at CHF. The increase in CHF with increased thickness of the Cu micro-porous surface layers could be attributed to an increase in the wetted surface area because of the developed hemi-spherical depression in the Cu micro-porous surface layers during the 2nd stage of deposition, as shown the SEM images in Figs. 3–7 and 19.

6. Summary and conclusions

Enhancement of saturation nucleate boiling of PF-5060 dielectric liquid on structurally strengthened and conditioned Cu micro-porous layers of different thickness and surface morphology is investigated. The five layers investigated (95, 139, 171, 197 and 220-μm thick) are deposited on 10×10 mm and 1.38–1.6-mm thick Cu substrates using a two-stage electrochemical process. The basic Cu dendrites micro-structure and the layer thickness are developed in the first stage of deposition using a current density of 3 A/cm^2 for 15–44 s, depending on the desired thickness. At the end of this stage, the deposited surfaces have large volume porosities (>90%) and orderly arranged open macro-pores surrounded by dense, but fine and branching Cu dendrites (Fig. 19). This micro-structure is structurally strengthened by continuing the electrochemical disposition using much lower current density for a second stage that lasted 10's of minutes. During this stage, the surface layer thickness insignificantly changes, but the dendrites micro-structure is masked by clusters of Cu micro-particles and some of the surface macro-pores are filled up with depositing Cu

atoms and micro-particles. Thus, the second stage of electrochemical deposition effectively reduces the volume porosity (65–80%), changes the surface morphology and increases the wetted surface area (Figs. 3b–7b).

When the structurally strengthened Cu micro-porous surface layers are used in the boiling experiments for the first time, the boiling curve in successively performed boiling tests shifted toward higher surface superheats. After a few (2–3) boiling tests, the surface layers become conditioned and the pool boiling curves become highly reproducible. For the conditioned micro-porous surface layers, there is either no or small temperature excursion prior to boiling incipience (<7 K). The present saturation CHF values of PF-5060 liquid on the Cu micro-porous layers deposited and investigated in this work (22.7–27.8 W/cm^2) and those of h_{MNB} (2.05–13.5 W/cm^2 K) are ~40–70% higher than and more than 17 times those reported for FC-72 on plane surfaces (<16 W/cm^2 and ~0.8 W/cm^2 K). The present results are markedly better than those reported by various investigators for saturation boiling of PF-5060 and FC-72 dielectric liquids on roughened plane, micro-porous and micro- and macro-structured surfaces, metal foams and on surfaces with micro-porous coatings.

The electrochemical process used to deposit the Cu micro-porous surface layers is relatively simple, inexpensive, and widely used in many commercial applications. The adhesion to the Cu substrates and the handling of the Cu micro-porous surface layers during the assembly of the test sections and conduct of the pool boiling experiments are good. Ongoing work is investigating the effects of surface orientation and liquid subcooling on the total thermal power removed by nucleate boiling on the Cu micro-porous layers and on the values of CHF and h_{MNB} and the corresponding surface superheats.

The present saturation boiling heat transfer results for PF-5060 dielectric on the Cu micro-porous surface layers #2 and #3 (Table 1 and Fig. 17a and b) are very promising for potential applications of cooling high power chips and CPUs, while keeping the junctions' temperature relatively low (<60 °C). The nucleate boiling results for the 171-μm thick, surface layer #3 are the best: saturation CHF of 27.8 W/cm^2 occurs at ΔT_{sat} of only 2.16 K and h_{MNB} of 13.5 W/cm^2 K occurs at ΔT_{sat} of only 2.0 K. The second best results are on surface layer #2: the saturation CHF and h_{MNB} of 24.54 W/cm^2 and 9.25 W/cm^2 K occur at ΔT_{sat} = 3.06 and 2.8 K, respectively. For future cooling and boiling heat transfer applications, additional research is needed to investigate the effects of fouling and aging of the Cu dendrites micro-porous layers on nucleate boiling heat transfer and CHF and the techniques for the deposition of metal micro-porous layers on larger surfaces than used in the present work.

Acknowledgement

This research is funded by the University of New Mexico's Institute for Space and Nuclear Power Studies.

References

3M, 2009a. Fluorinet Electronic Liquids FC-72, Products Information. <http://www.3m.com/>.
3M, 2009b. Performance Fluid PF-5060, Products Information. <http://www.3m.com/electronicmaterials>.
3M, 2009c. Novec Engineering Fluid HFE-7100 for Heat Transfer. <http://www.3m.com/electronicmaterials>.
Albertson, C.E., 1977. Boiling heat transfer surface and method. US Patent 4018,264.
Chang, J.Y., You, S.M., 1996. Heater orientation effects on pool boiling on micro-porous enhanced surfaces in saturated FC-72. J. Heat Transf. 118, 937–943.
Chang, J., You, S.M., Haji-Sheikh, A., 1998. Film boiling incipience at the departure from natural convection on flat, smooth surfaces. J. Heat Transf. 120, 402–409.
Chih, K., Lu, Yu, D.C., 2007. Pool boiling heat transfer on horizontal rectangular fin array in saturated FC-72. Int. J. Heat Mass Transf. 50, 3624–3637.
El-Genk, M.S., Ali, A.F., 2010a. Saturation and subcooled boiling on copper nanodendrite surfaces. In: Proceedings 14th International Heat Transfer Conference, Paper# IHTC14-22108, Washington DC, 8–13 August 2010.
El-Genk, M.S., Ali, A.F., 2010b. Enhancement of saturation boiling of PF-5060 on micro-porous copper dendrites surfaces. J. Heat Transf. 132, 071501-1–071501-9.
El-Genk, M.S., Bostanci, H., 2003. Saturation boiling of HFE-7100 from a copper surface, simulating a microelectronic chip. Int. J. Heat Mass Transf. 46, 1841–1854.
El-Genk, M.S., Parker, J.L., 2008. Nucleate boiling of FC-72 and HFE-7100 on porous graphite at different orientations and liquid subcooling. J. Energy Convers. Manage. 49, 733–750.
Furberg, R., 2006. Enhanced Boiling Heat Transfer from a Novel Nanodentritic Microporous Copper Structure. Ph.D. Dissertation. KTH School of Industrial Engineering and Management, Stockholm, Sweden.
Furberg, R., Li, S., Palm, B., Toprak, M., Muhammed, M., 2006. Dendritically ordered nano-particles in a micro-porous structure for enhanced boiling. In: Proceedings 13th International Heat Transfer Conference, Paper No. NAN-07, Sydney, Australia.
Ghiu, C.-D., 2007. Pool Boiling from Enhances Structure under Confinement. Ph.D. Dissertation. Georgia Institute of Technology, USA.
Jiang, Y.Y., Wang, W.C., Wang, D., Wang, B.X., 2001. Boiling heat transfer on machined porous surfaces with structured optimization. Int. J. Heat Mass Transf. 44, 443–456.
Jung, J.-Y., Kwak, H.-Y., 2006. Effect of surface condition on boiling heat transfer from silicon chip with submicron-scale roughness. Int. J. Heat Mass Transf. 49, 4543–4551.
Kim, J.H., 2006. Enhancement of Pool Boiling Heat Transfer using Thermally-conductive Microporous Coating Techniques. Ph.D. Dissertation. UT, Arlington, TX.
Kim, J., 2009. Review of nucleate pool boiling bubble heat transfer mechanisms. Int. J. Multiphase Flow 35, 1067–1076.
Kim, J.H., Kashinath, M.R., Kwark, S.M., You, S.M., 2007. Optimization of microporous structures in enhanced pool boiling heat transfer of saturated R-123, FC-72, and water. In: Proc. ASME-JSME Thermal Engineering Summer Heat Transfer Conference, HT2007-32339.
Kim, Y.-Ho, Lee, K.-J., Han, D., 2008. Pool boiling enhancement with surface treatments. J. Heat Mass Transf. 45, 55–60.
Kline, S.J., 1985. The purposes of uncertainty analysis. Trans. ASME J. Fluids Eng..
Launay, S., Fedorov, A.G., Joshi, Y., Gao, A., Ajayan, P.M., 2006. Hybrid micro-nano structured thermal interfaces for pool boiling heat transfer enhancement. Microelectron. J. 37, 1158–1164.
Li, S., Furberg, R., Toprak, M.S., Palm, B., Muhammed, M., 2008. Nature-inspired boiling enhancement by novel nanostructure macroporous surfaces. Adv. Funct. Mater. 18, 1–6.
Nimkar, N.K., Bhavnani, S.H., Jaeger, R.C., 2006. Benchmark heat transfer date for microstructured surfaces for immersion-cooled microelectronics. IEEE Trans. Compon. Packag. Technol. 29, 89–97.
Parker, J.L., El-Genk, M.S., 2005. Enhanced saturation and subcooled boiling of FC-72 dielectric liquid. Int. J. Heat Mass Transf. 48, 3736–3752.
Parker, J.L., El-Genk, M.S., 2006. Effect of surface orientation on nucleate boiling of FC-72 on porous graphite. J. Heat Transf. 128, 1159–1175.
Parker, J.L., El-Genk, M.S., 2009. Saturation boiling of HFE-7100 dielectric liquid on copper surfaces with corner pins at different inclinations. J. Enhanced Heat Transf. 116, 103–122.
Rainey, K.N., You, S.M., 2000. Pool boiling heat transfer from plain and micro-porous, square pin-finned surfaces in saturated FC-72. J. Heat Transf. 122, 509–516.
Rajalu, K.G., Kumar, R., Mohanty, B., Varma, H.K., 2004. Enhancement of nucleate pool boiling heat transfer coefficient by reentrant cavity surfaces. Heat Mass Transf. 41, 127–132.
Ramaswamy, C., Joshi, Y., Nakayama, W., Johnson, W.B., 2003. Effects of varying geometrical parameters on boiling from microfabricated enhanced structures. J. Heat Transf. 125, 103–109.
Shin, H.C., Liu, M., 2004. Copper foam structures with highly porous nanostructured walls. Chem. Mater. 16, 5460–5464.
Shin, H.C., Dong, J., Liu, M., 2003. Nanoporous structure prepared by an electrochemical deposition processes. Adv. Mater. 15, 1610–1614.
Sriraman, S.R., Banerjee, D., 2007. Pool boiling studies on nano-structured surfaces. In: ASME Int. Mechanical Engineering Congress and Exposition, Paper # IMECE2007-42581, Seattle, USA.
Vemuri, S., Kim, K.J., 2005. Pool boiling of saturated FC-72 on nano-porous surface. Int. Commun. Heat Mass Transf. 32, 27–31.
Webb, R.L., 2004. Odyssey of the enhanced boiling surface. J. Heat Transf. 126, 1051–1059.
Wei, J.J., Honda, H., 2003. Effect of fin geometry on boiling heat transfer from silicon chips with micro-pin-fins immersed in FC-72. Int. J. Heat Mass Transf. 46, 4059–4070.
Xu, J., Ji, X., Zhang, W., Liu, G., 2009. Pool boiling heat transfer of ultra-light copper foam with open cells. Int. J. of Multiphase Flow 34, 1008–1022.
Yu, C.K., Lu, D.C., 2007. Pool boiling heat transfer on horizontal rectangular fin array in saturated FC-72. Int. J. Heat Mass Transf. 50, 3624–3637.
Yu, C.K., Lu, D.C., Cheng, T.C., 2006. Pool boiling heat transfer on artificial micro-cavity surfaces in dielectric fluid FC-72. J. Michromech. Microeng. 16, 2092–2099.